NON-LINEAR, LOW ORDER INTERACTIONS

A.C. Wiin-Nielsen

and

E. Källén

European Centre for Medium
Range Weather Forecasts,
England

Seminar, 1979

1. INTRODUCTION

The European Centre for Medium Range Weather Forecasts is an intergovernmental institution devoted to weather forecasts for periods up to 10 days. The Centre has recently started its first operational phase, and we are starting to issue forecasts to the Member States on an experimental basis. The present operational weather prediction model and the other models available at the Centre are developed using the best available parameterisation schemes and the numerical schemes which in our experience function well and have good accuracy. It is obvious that the staff of the Centre has drawn heavily on the research work done in the past by the meteorologists who developed the methods for short-range prediction and for simulations of the general circulation of the atmosphere. These developments are in turn based on our present knowledge of the dynamics and thermodynamics of the atmosphere. It is thus seen that a further improvement of the medium-range prediction models depends ultimately on an increase in our understanding of the dynamics of the atmospheric processes. Due to this fact it is entirely appropriate that the annual seminar is devoted to dynamical meteorology and numerical weather prediction.

The concept of scale has been extremely useful in the development of numerical weather prediction. The observing network - inhomogeneous as it is - defines at most the large scale motion of the atmosphere, while the micro- and meso-scale motion almost by definition cannot be resolved by the synoptic network. We are therefore resigned to the fact that only the large-scale motion and structure can be predicted directly and explicitly by our models. We know also that many of the physical processes in the atmosphere are of a microphysical nature (radiation, condensation, evaporation, precipitation, convection etc.). For the dynamicist who wants to

contribute to the development of a prediction model it is not only required that he must understand the basic dynamics of a given physical process, but he must also be able to express the essential parts of the dynamics in terms which involve the large scale parameters carried in the model (parameterisation).

The prediction model designer should for each physical process - to the extent it can be considered in isolation - decide :

(i) whether or not the dynamics of the process is known

(ii) whether or not the effects of the process influences the large scale state of the atmosphere, and, if so,

(iii) how can the essential dynamics be expressed in terms of the parameters used in the model.

This chain of events, although logically simple, represents nevertheless some of the most difficult problems in meteorology. I am personally convinced that the improvement of our models in the future to a large extent depends on our ability to make realistic parameterisation schemes for the physical processes of the atmosphere. This statement applies particularly to medium-range forecasts.

In the following sections we shall discuss some of the basic aspects of the medium-range prediction problem and other related problems in atmospheric dynamics.

2. NON-LINEAR INTERACTIONS

In inspecting the programme for this seminar it is unavoidable to notice that many of the contributions deal with linear or quasi-linear problems. While I agree that much can be learned from linear equations, and that these equations due to the state of the art in mathematics are just about the only equations from which solutions can be obtained, we must nevertheless remember that very important aspects of atmospheric dynamics is basically non-linear. To remind all of us about this fact I reproduce a summary of calculations recently carried out by Chen and Wiin-Nielsen (1978). We calculated the non-linear interaction of kinetic energy I_n, of enstrophy J_n, and of available potential energy L_n from atmospheric data (10 levels, December 19, 1971 - February 27, 1972, 00 and 12 GMT). The results are displayed in our paper as a function of the meridional index n, but here we shall be satisfied with a summary where the results have been grouped as follows: $1 \leqslant n \leqslant 7$, $8 \leqslant n \leqslant 14$, $15 \leqslant n \leqslant 31$. Table 1 shows the results.

Table 1

n	I_n, erg cm^{-2} s^{-1}	J_n, 10^{-18} s^{-3}	L_n, erg cm^{-2} sec^{-1}
1 - 7	830	39	-3786
8 - 14	-877	-328	2604
15 - 31	47	289	1182

Table 1 shows at a glance that the non-linear transfer of available potential energy is from the larger scale (mainly n=2) to the medium and shorter scales while the kinetic energy and the enstrophy are transferred from the middle scale where they are created by conversion from available potential energy to the larger and smaller scales. In agreement with Fjørtoft's (1953) theoretical

deductions the larger fraction of the kinetic energy is transferred to the large scale while the larger fraction of the enstrophy is transferred to the small scale.

These recent results are of course only confirming earlier results obtained by Steinberg, Wiin-Nielsen and Yang (1971), Saltzman (1970) and Yang (1967), but the most recent results are the first which use the spectral index n as the scale parameter.

The non-linear interactions are not negligible as compared to other energy parameters. A useful yardstick is the estimated total energy conversion from available potential energy to kinetic energy which is about 5 Wm^{-2} = 5000 erg cm^{-2} s^{-1}. It is thus seen that the non-linear interactions must be included somehow in any realistic model of dealing with the various scales of motion.

It has been suggested from time to time that it should be attempted to formulate a numerical model which describes the large scales only. This suggestion makes sense because the large scale motion defines the major waves which in turn determine the type of weather in a given geographical region. The results displayed here show that such a model must contain a correct parameterization of the interaction between the large scale and all the other scales. No successful parameterization of the non-linear transfer has been made so far.

3. A VERY SIMPLE NONLINEAR MODEL

Continuing on the theme of nonlinear behaviour I shall next demonstrate some recent results obtained in collaboration with E. Källén and so far unpublished. We have elaborated on some results obtained by me in 1975 and published in the proceedings of the first ECMWF seminar. In some areas we have even succeeded in generalising the early results.

The basic equation is the advective equation with forcing and dissipation, i.e.

$$\frac{\partial u_*}{\partial t_*} + u_* \frac{\partial u_*}{\partial x_*} = - \varepsilon u_* + B(u_{E*} - u_*) \qquad (3.1)$$

Without forcing and dissipation this equation is energy but not enstrophy conserving.

The equation (3.1) is transformed into the spectral domain by considering a distance $0 \leqslant x_* \leqslant L$, and $u_* = 0$ for $x_* = 0$, $x_* = L$. In this case we can use an expansion in sine-functions only. After expansion in the spectral domain, after non dimensionalisation, and after reduction to a two-component system, where $U(1) = x$ and $U(2) = y$, we have the equations

$$\frac{dx}{dt} = \frac{1}{2} xy - x + x_E$$

$$\frac{dy}{dt} = - \frac{1}{2} x^2 - y + y_E \qquad (3.2)$$

The two-component system is possible, because the basic system has only one conservative property.

(3.2) is the system considered in 1975. At that time the whole investigation was limited to the case $x_E = 0$ and $y_E \neq 0$. We shall now consider the general case where $x_E \neq 0$ and $y_E \neq 0$.

The first problem is to find the steady states, i.e. those states where dx/dt = dy/dt = 0.

Denoting a steady state by (x_s, y_s) we find that all steady states are solutions to the equations

$$\frac{1}{2} x_s (y_s - 2) + x_E = 0$$
$$-\frac{1}{2} x_s^2 - y_s + y_E = 0 \qquad (3.3)$$

leading to the equation

$$x_s^3 - 2(y_E - 2) x_s - 4 x_E = 0 \qquad (3.4)$$

The equations (3.3) may be considered as curves in the (x_s, y_s) plane. The steady states are given by the intersections of these curves. The parabola in Figure 1 represents the curve dy/dt = 0, while the hyperbola corresponds to dx/dt = 0. y_E determines the maximum of the parabola while x_E determines the shape of the hyperbola. It is thus seen that when y_E is smaller than a certain critical value there is only one intersection between the curves, i.e. one steady state. Three intersections (three steady states) will exist when y_E is larger than the critical value. The critical value is x_E dependent and we must thus investigate the number of real roots in (3.4). They are determined by the quantity

$$\Delta = 4(x_E^2 - \frac{2}{27} (y_E - 2)^3) \qquad (3.5)$$

according to the classical theory of the cubic equation. $\Delta < 0$ indicates three real roots. $\Delta > 0$ is the case of one real and two complex roots. Three steady states exist

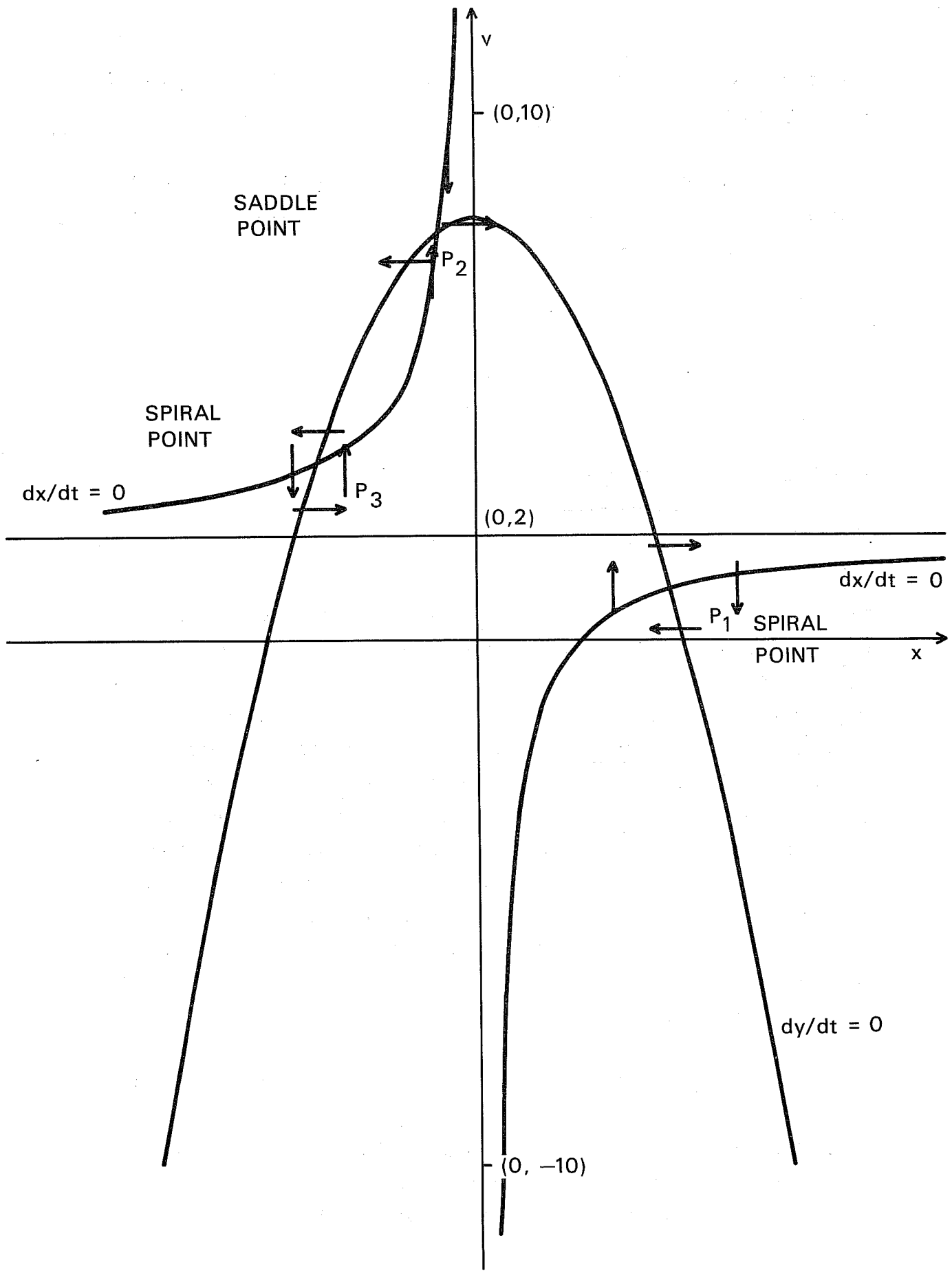

Fig. 1 Representation of the steady states P_1, P_2 and P_3. The parabola is the curve on which dy/dt = 0, while dx/dt = 0 on the hyperbola. The horizonal line through (0,2) is an asymptote for the hyperbola. The intersections are the steady states. The arrows indicate the direction of the trajectory at points on the parabola or the hyperbola as deduced from the basic equations.

thus when

$$|x_E| < \left[\frac{2}{27}\,(y_E - 2)^3\right]^{\frac{1}{2}} \tag{3.6}$$

(3.6) can be satisfied only if $y_E > 2$.

The values of the three real roots are

$$x_{sj} = 2\sqrt{\frac{2(y_E-2)}{3}}\,\cos\,(\tfrac{1}{3}\phi + j\cdot\tfrac{2\pi}{3}),\ j=0,1,2 \tag{3.7}$$

where ϕ is evaluated from the expression

$$\cos\phi = \frac{x_E}{\sqrt{\frac{2}{27}(y_E-2)^3}} \tag{3.8}$$

Returning to Figure 1 which corresponds to the case of 3 steady states we may investigate the trajectories in the immediate neighborhood of the three intersections P_1,P_2 and P_3. Using the basic equations for the system and the facts that dx/dt = 0 on the hyperbola and dy/dt = 0 on the parabola we may deduce the direction of the trajectory in four points surrounding the steady state. In this way we find that P_1 and P_3 are so-called spiral points, while P_2 is a saddle point. P_2 is therefore an unstable steady state, while P_1 and P_3 may be stable or unstable depending on whether the spiral approaches the steady state or goes away from it. This question can be settled by a linear stability analysis.

We consider therefore an arbitrary steady state (x_s, y_s). Linearising the basic equations we get

$$\frac{dx'}{dt} = \frac{1}{2} x_s y' + \frac{1}{2} y_s x' - x'$$

$$\frac{dy'}{dt} = - x_s x' \qquad - y' \tag{3.9}$$

where perturbation quantities are denoted by primes. We seek solutions of the form

$$(x',y') = (x_o,y_o)e^{\sigma t} \tag{3.10}$$

where σ is the eigenvalue. $\sigma_r > 0$ indicates instability. Using the usual procedure of substituting (3.10) in (3.9) and finding the conditions for nontrivial solutions by setting the determinant to zero we find that

$$\sigma = \frac{1}{4}\left[(y_s - 4) \pm \sqrt{y_s^2 - 8x_s^2}\right] \tag{3.11}$$

Considering first the region in which $y_s^2 < 8x_s^2$ we find that $\sigma_r > 0$ if $y_s > 4$. On the other hand, if $y_s^2 > 8x_s^2$, then σ is real. σ will certainly be positive if $y_s > 4$. In addition, σ will be positive for $y_s < 4$ if

$$y_s^2 - 8x_s^2 > (4 - y_s)^2 \tag{3.12}$$

or

$$y_s > x_s^2 + 2 \tag{3.13}$$

Figure 2 shows the stable and unstable regions in the (x_s, y_s) plane. It is naturally preferable to express the stability criteria

$$x_s^2 + 2 < y_s < 4 \text{ and } y_s > 4 \tag{3.14}$$

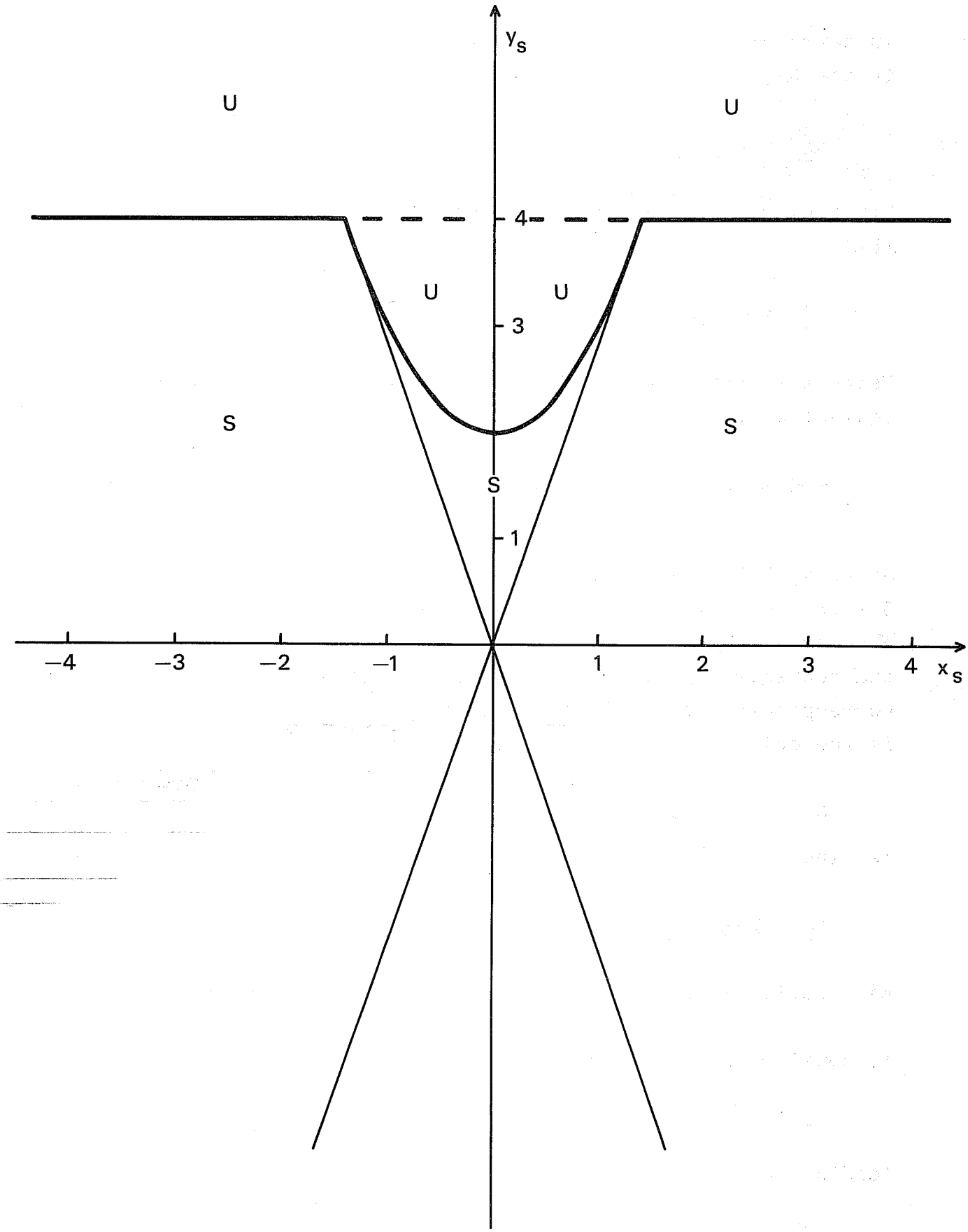

Fig. 2 The stability diagram in the (x_s, y_s) plane. The straight lines through the origin are $y_s = \pm 2\sqrt{2}\, x_s$. U and S indicate unstable and stable regions, respectively.

in terms of x_E and y_E and to derive a stability diagram in the (x_E, y_E) plane. We consider first the region

$$x_s^2 + 2 < y_s < 4 \tag{3.15}$$

Since $y_E = y_s + \frac{1}{2} x_s^2$ we find that $2 < y_E < 5$ and furthermore that

$$x_s^2 < \frac{2}{3} (y_E - 2) \tag{3.16}$$

Using the expression (3.7) for x_s we find that (3.16) is equivalent to

$$-\frac{1}{2} < \cos(\frac{1}{3}\phi + j\,\frac{2\pi}{3}) < \frac{1}{2} \tag{3.17}$$

Since $x_E > 0$ it follows that $0 < \phi < \frac{1}{2}\pi$ and thus $0 < \frac{1}{3}\phi < \frac{1}{6}\pi$. It is thus easy to see that the roots corresponding to $j = 0$ and $j = 1$ do not satisfy (3.17) and consequently are stable steady states while the root corresponding to $j = 2$ does satisfy (2.17) and therefore is the only unstable steady state. From

$$0 < \cos\phi < 1$$

we find that

$$x_E < \sqrt{\frac{2}{27} (y_E-2)^3}, \quad 2 < y_E < 5 \tag{3.18}$$

as a region with one unstable and two stable steady states.

We consider next the region

$$y_s > 4 \tag{3.19}$$

leading to

$$x_s^2 < 2(y_E - 4); \quad y_E > 4 \tag{3.20}$$

Using again (3.7) for x_s we find from (3.20) that it leads to the inequalities

$$-\sqrt{\frac{3}{4}\frac{y_E^{-4}}{y_E^{-2}}} < \cos\left(\frac{1}{3}\phi + j\,\frac{2\pi}{3}\right) < \sqrt{\frac{3}{4}\frac{y_E^{-4}}{y_E^{-2}}} \tag{3.21}$$

It is convenient to define the angle θ by

$$\cos\theta = \sqrt{\frac{3}{4}\frac{y_E^{-4}}{y_E^{-2}}}\ ; \quad 0 \leqslant \theta \leqslant \frac{\pi}{2} \tag{3.22}$$

and we get from (3.21) that it will be satisfied if

$$\theta < \frac{1}{3}\phi + j\,\frac{2\pi}{3} < \pi - \theta \tag{3.23}$$

or

$$\pi + \theta < \frac{1}{3}\phi + j\,\frac{2\pi}{3} < 2\pi - \theta \tag{3.24}$$

The object is now to investigate if the three roots satisfy either (3.23) or (3.24). We start by noting from (3.22) that the right hand side will vary monotonically between 0 for $y_E = 4$ and $\frac{1}{2}\sqrt{3}$ for y_E approaching infinity. It follows that

$$\frac{1}{6}\pi < \theta < \frac{1}{2}\pi \tag{3.25}$$

Considering first the case j=0 we have

$$0 < \frac{1}{3}\phi < \frac{1}{6}\pi < \theta \tag{3.26}$$

showing that the first steady state is stable.

For j = 1 we find

$$\frac{2}{3}\pi < \frac{1}{3}\phi + \frac{2\pi}{3} < \frac{5\pi}{6} \tag{3.27}$$

If $\frac{1}{3}\phi + \frac{2}{3}\pi$ shall be in the interval $[\theta, \pi-\theta]$ we must require that

$$\frac{1}{3}\phi + \frac{2}{3}\pi < \pi-\theta$$

or

$$\phi < \pi - 3\theta \tag{3.28}$$

Since ϕ is positive it is seen that (3.28) cannot be satisfied if

$$\pi - 3\theta < 0 \tag{3.29}$$

leading to

$$\cos\theta < \frac{1}{2} \tag{3.30}$$

and therefore

$$y_E < 5 \tag{3.31}$$

The second steady state is therefore stable for $y_E < 5$. For $y_E > 5$ we find that (3.28) will be satisfied if

$$x_E > -\sqrt{\frac{2}{27}(y_E-2)^3}\cos\left[3\arccos\sqrt{\frac{3}{4}\frac{y_E-4}{y_E-2}}\right] \tag{3.32}$$

The second steady state is therefore unstable if $y_E > 5$ and (3.32) is satisfied.

For j = 2 we have

$$\frac{4}{3}\pi < \frac{1}{3}\phi + \frac{4}{3}\pi < \frac{3}{2}\pi \tag{3.33}$$

If $\frac{1}{3}\phi + \frac{4}{3}\pi$ shall be in the interval $[\pi + \theta, 2\pi - \theta]$ we must require

$$\pi + \theta < \frac{1}{3}\phi + \frac{4}{3}\pi$$

or

$$\phi > 3\theta - \pi \tag{3.34}$$

(3.34) is always satisfied if $3\theta - \pi < 0$ leading to

$$y_E > 5 \tag{3.35}$$

The third steady state is thus unstable if $y_E > 5$. For $y_E < 5$ we must require that (3.34) is satisfied leading to

$$x_E < -\sqrt{\frac{2}{27}(y_E-2)^3}\cos\left[3\arccos\sqrt{\frac{3}{4}\frac{y_E-4}{y_E-2}}\right] \tag{3.36}$$

The results of these analyses are summarised in Figure 3 showing the regions in which the second and third steady states are unstable.

In the calculations above we have considered the case of three steady states. We shall finally consider the case when only one steady state exists. As shown below this state is always stable. The region of our steady state in the (x_E, y_E) plane is given by

$$x_E^2 > \frac{2}{27}(y_E-2)^3 \tag{3.37}$$

Since

$$y_E = y_s + \frac{1}{2} x_s^2$$
$$x_E = -\frac{1}{2} x_s (y_s - 2) \qquad (3.38)$$

we find after some calculations that (3.37) in the (x_s, y_s) plane can be written in the form

$$(y_s - 2 - x_s^2)^2 \; (8(y_s - 2) + x_s^2) < 0 \qquad (3.39)$$

(3.37) corresponds therefore in the (x_s, y_s) plane to the region

$$y_s < 2 - \frac{1}{8} x_s^2 \qquad (3.40)$$

which is entirely in the stable region of Figure 2.

The stability analysis in this section may be repeated for $x_E < 0$. The result is a stability diagram symmetrical to the diagram in Figure 3 around the y_E - axis. The dashed curve in Figure 3 will be explained below.

Figure 3 shows that in the region of three steady states there are two very different sub-regions. The region to the right hand side, i.e. for large values of x_E and y_E, is characterised by 2 unstable and 1 stable steady state. It is to be expected and numerical experiments have confirmed that the single stable steady state is the asymptotic state, or, in other words, all trajectories wherever they start will eventually approach the stable steady state. The remaining part of the region is characterised by 1 unstable and 2 stable steady states. In this case we know only that if we start a trajectory close to the unstable steady state it will move away from the state, but the linear stability analysis cannot tell us which steady

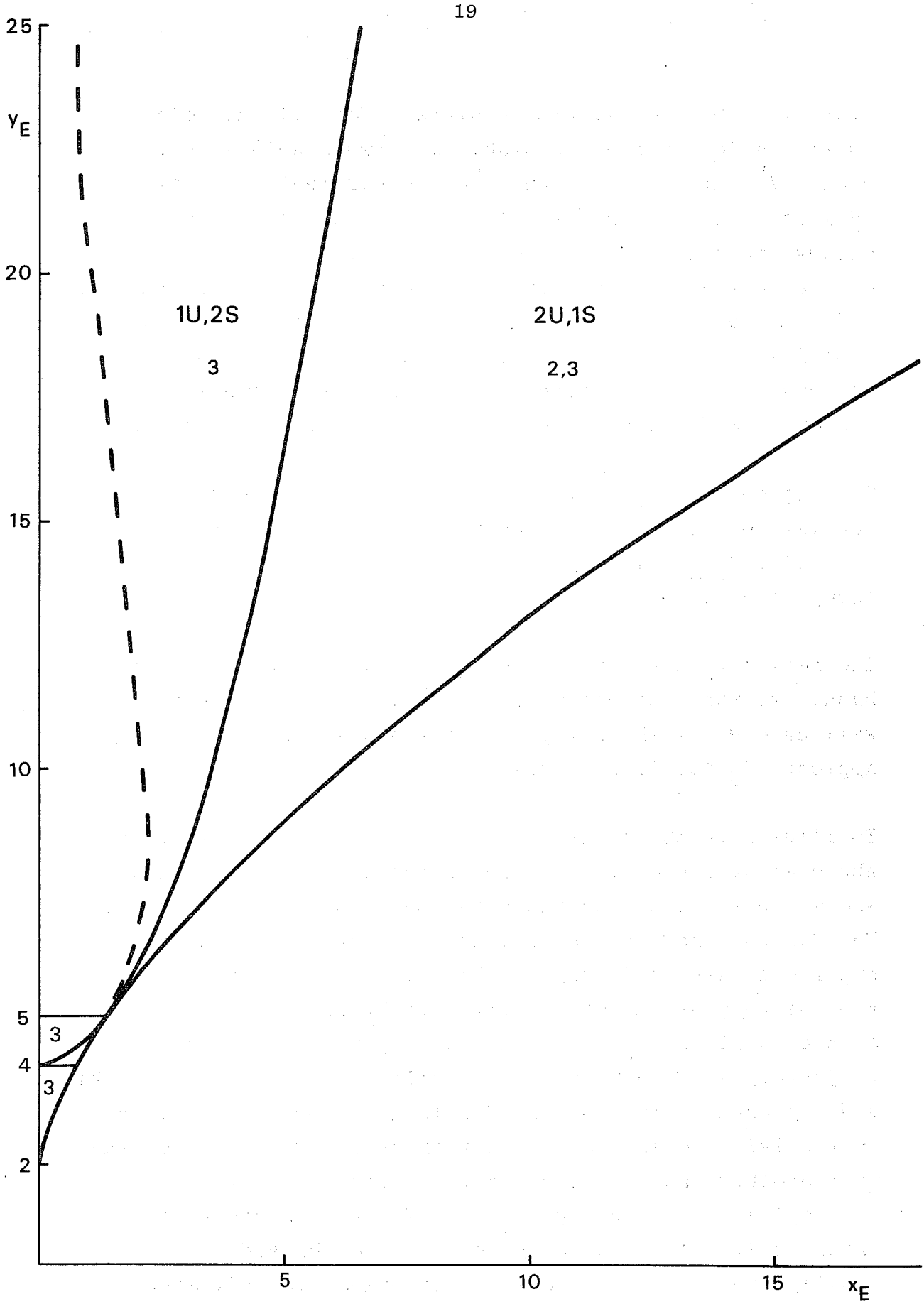

Fig. 3 The stability diagram in the (x_E, y_E) plane. The lower curve separates the region of one stable steady state below and three steady states above. The other full curve from $(\sqrt{2}, 5)$ upwards separates the region to the left of one unstable and two stable steady states and the region to the right of the two unstable and one stable steady state. The dashed curve, determined by numerical experiments, separates the regions with and without "limit cycles".

state will be the asymptotic state. For all the points in the region with one unstable and two stable steady states we carried out a numerical experiment. We selected 36 initial states on a small circle with the unstable steady state as centre. For each initial state we carried out a numerical integration until a steady state was reached. Based upon the results of these numerical experiments it is possible to sub-divide the region of one unstable and two stable steady states in two sub-regions sub-divided by the dashed line entered on Figure 3.

The region to the right of the dashed line in Figure 3 consists of points where all the trajectories surrounding the point P_2 in Figure 1 will have the point P_1 as the asymptotic steady state.

The region to the left of the dashed line, on the other hand, are those points where some of the trajectories will have P_1 as the asymptotic state while others approach P_3 for large times.

To illustrate the behaviour in some of the cases mentioned above we have prepared the following figures. Figure 4 shows a case of two unstable and one stable steady state. The dashed lines in Figure 4 show the parabola and the hyperbola used in Figure 1. In this case both P_2 and P_3 are unstable steady states although P_2 is an unstable saddle point and P_3 is an unstable spiral point. A trajectory starting close to P_2 will either go to the right and approach P_1 in a spiral for large times or it will go to the left, go around P_3 and then approach P_1 in a spiral. On the other hand, a trajectory starting close to P_3 will spiral out, approach P_2, but since this state is unstable it will eventually deviate from P_2 and will finally approach P_1. These trajectories are indicated on Figure 4.

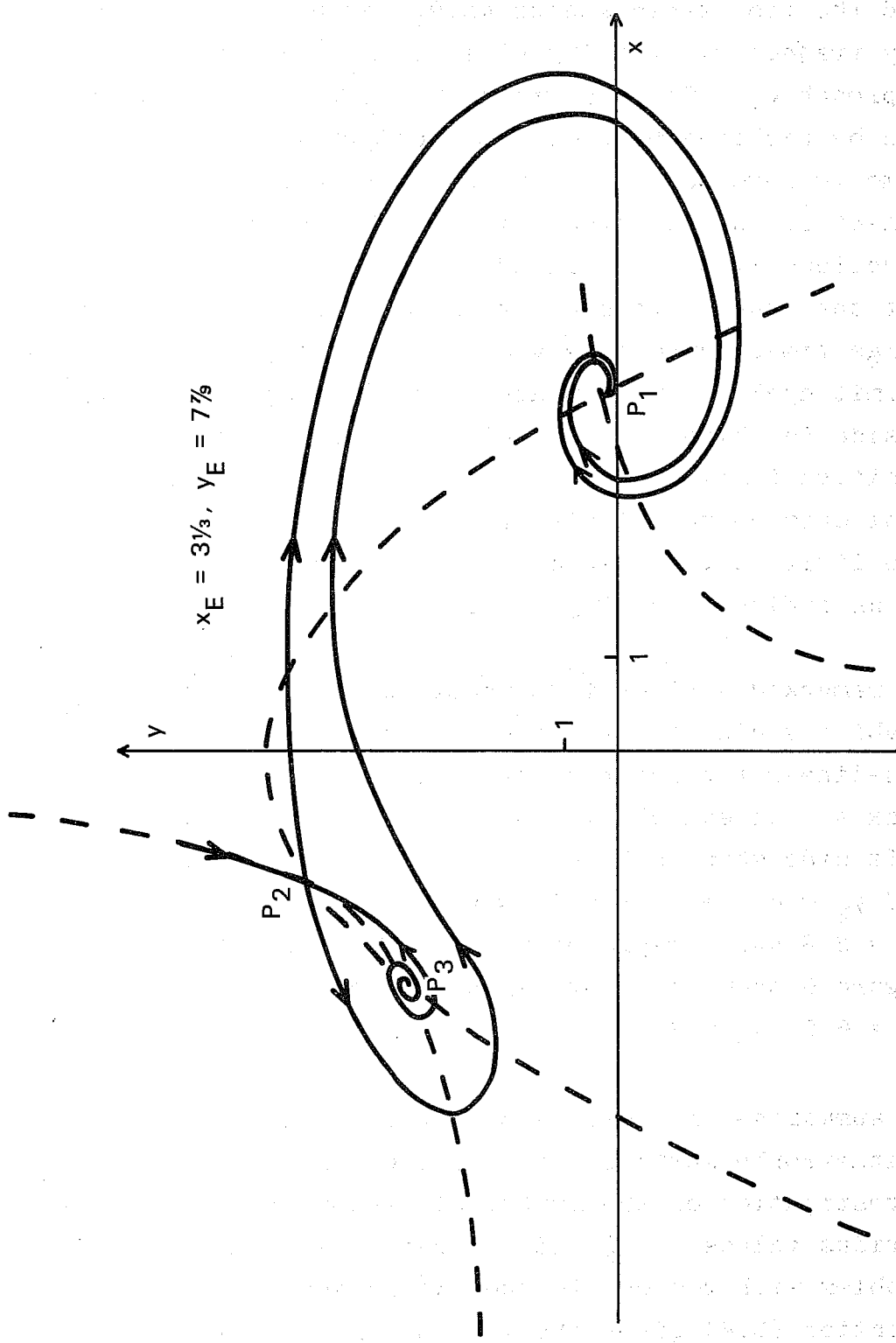

Fig. 4 Trajectories in the case two unstable steady states (P_2 and P_3) and one stable steady state (P_1). The dashed curves are the parabola and the hyperbola from Figure 1.

Figure 5 shows a case of one unstable and two stable steady states. The unstable steady state is as usual marked by P_2 and the two stable states as P_1 and P_3. It is seen that any trajectory starting close to P_2 will eventually approach P_1. The behaviour in the region surrounding P_3 can be explored by numerical integrations in which the time is reversed. An initial state close to P_3 is selected, and an integration of the basic nonlinear equations with t replaced by -t is carried out. It turns out that the "reversed" trajectory is a spiral which at large times approaches a curve, normally called an unstable "limit cycle". This means that any trajectory starting inside the "limit cycle" will approach P_3 for large positive times. On the other hand, a trajectory starting just outside the "limit cycle" will first depart from the limit curve, then approach P_2 and eventually come to P_1 as indicated on Figure 5.

We remarked earlier in connection with Figure 3 that the stability diagram is symmetric around the y_E-axis. The non-linear trajectories are also symmetrical around the y-axis. An example is shown in Figure 6 in which the left side shows a "limit cycle" calculated for $x_E = 1.9$ and $y_E = 6.0$ with the initial condition $x_o = -2.1$, $y_o = 3.8$ and t replaced by -t. The right hand side of Figure 6 shows the corresponding calculation for $x_E = -1.9$, $y_E = 6.0$, $x_o = 2.1$, $y_o = 3.8$.

To summarise the results obtained in this section a "catastrophe surface" for the model has been constructed. Investigation of the number of steady states obtained for various values of x_E and y_E, can be seen as a bifurcation problem with respect to the two parameters x_E and y_E. Equation (3.4) gives the form of the "catastrophe surface", and rewriting it as

$$x_E = \frac{x_s^3}{4} - \frac{x_s}{2}\ (y_E - 2) \qquad (3.41)$$

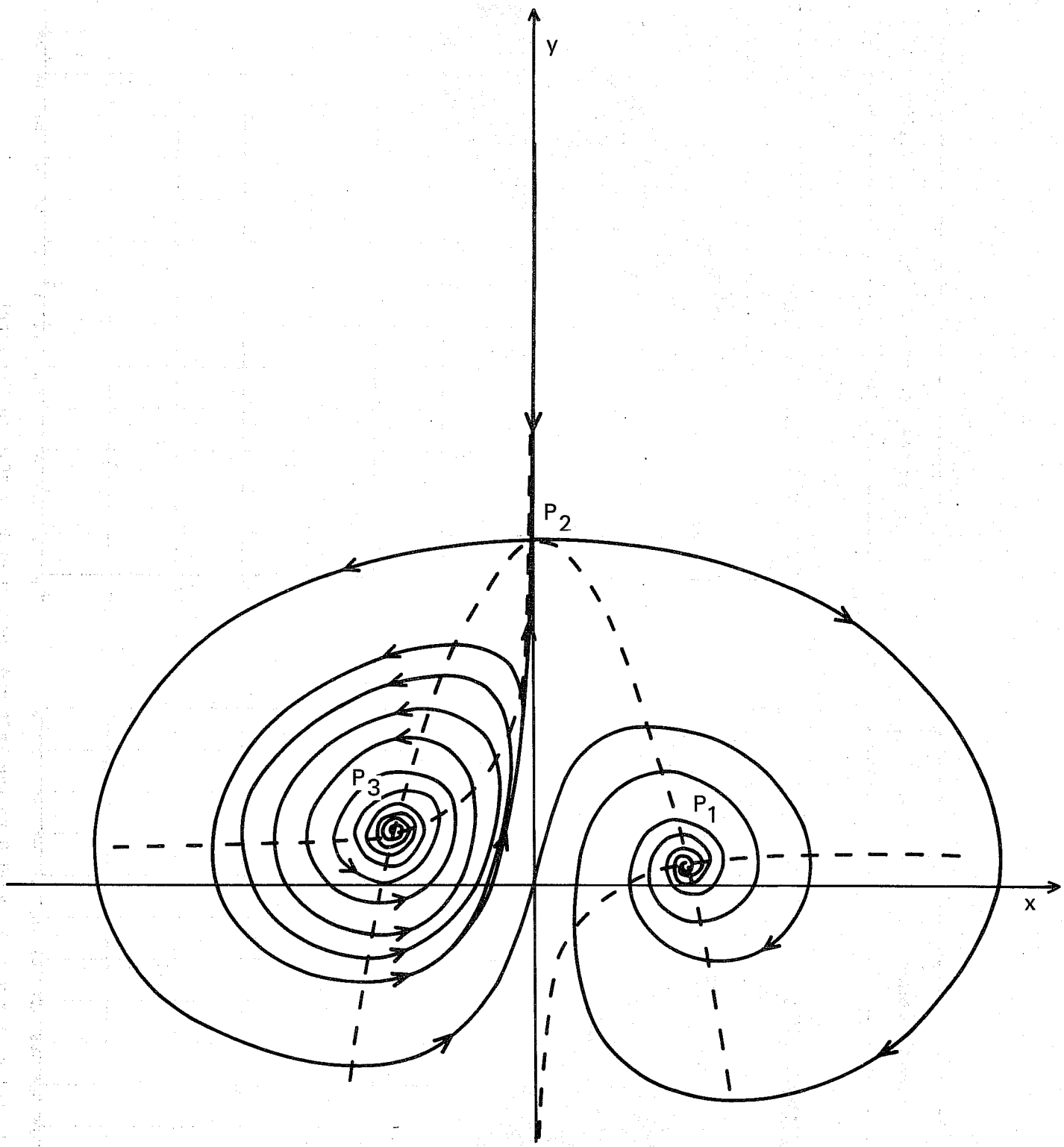

Fig. 5 Trajectories for the case $x_E = 3$, $y_E = 20$ with one unstable steady state P_2 and two stable steady states P_1 and P_3. The dashed curves are again the parabola and the hyperbola from Figure 1. P_3 is a stable spiral point surrounded by a "limit cycle" determined by a backward numerical integration.

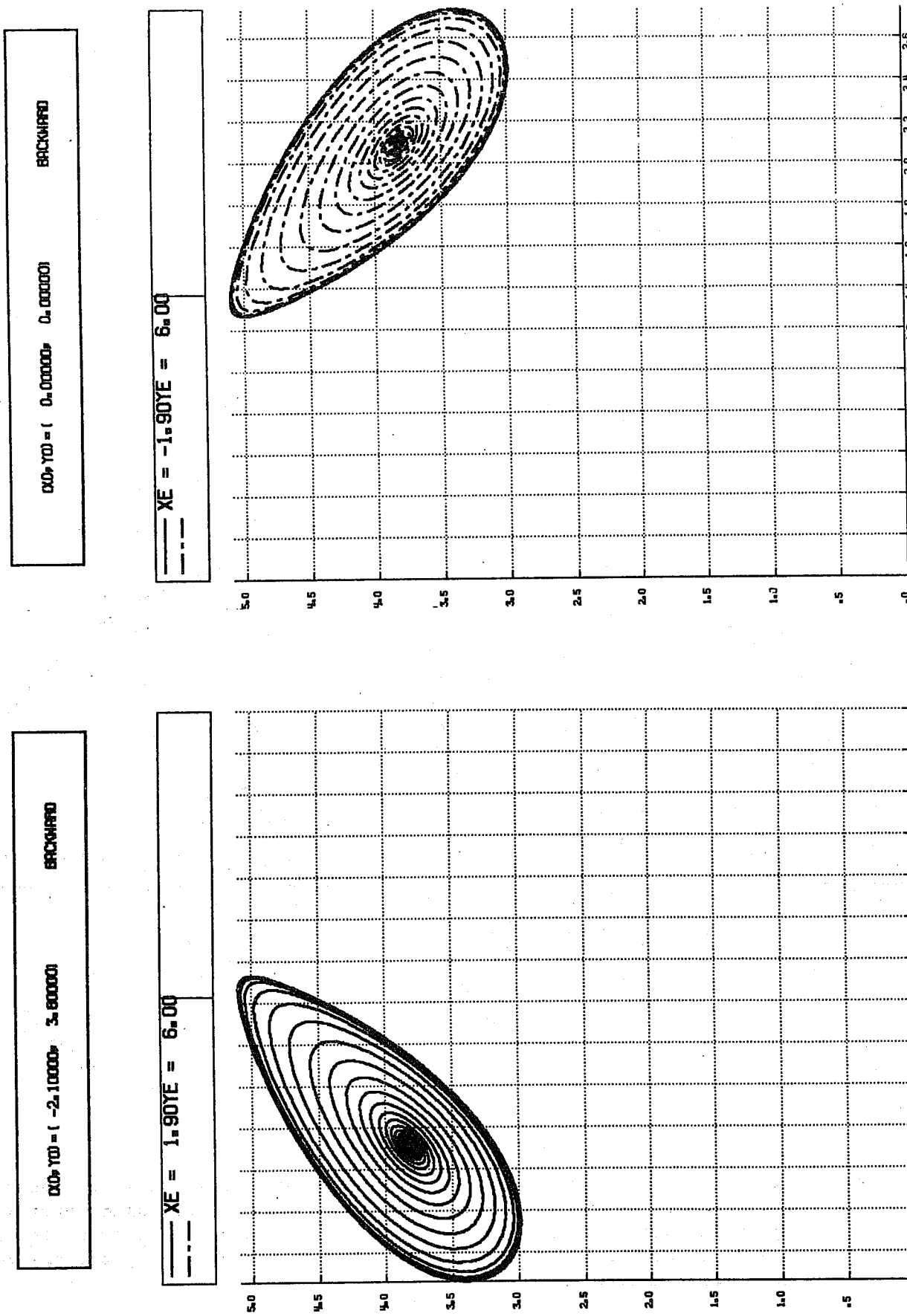

Fig. 6 "Limit cycles" for x_E=1.9, y_E=6.0 to the left and for x_E= -1.9, y_E=6.0 to the right. It it seen that there exists symmetry around the y-axis.

enables us to plot the surface. Figure 7 shows this surface from different angles of view. It can be seen from the figure that we have a cusp catastrophe, the bifurcation point occurring at $x_E = 0$, $y_E = 2$. For x_E- and y_E-values inside the cusp (bounded by the folds on the surface) we have three values of x_s for each pair of x_E, y_E, outside the cusp only one x_s is possible. Going back to Figure 3, the curve separating the regions of one and three steady states is a projection of the cusp on to the x_E, y_E-plane. The only difference is that Fig. 7 also involves negative x_E-values.

Looking at the catastrophe surface denoted 3731 0 0, we see the surface from above. The top pleat corresponds to the x_s-value of P_1 for a given value of (x_E, y_E). The bottom pleat is P_3, while the middle pleat (inside the fold) gives the x_s of P_2. As P_2 always is unstable, the middle pleat represents an unstable steady-state while the top and bottom pleats are unstable near the fold and stable further away from it. The unstable part of the top pleat is hatched in Figure 7.

The surface denoted 3731135-20 in Figure 7 shows the same catastrophe surface seen from another angle. The left hand upsloping side of the surface corresponds to the top pleat in the surface above, while the bottom pleat corresponds to the right hand downsloping side. On the bottom surface the middle pleat is clearly seen, while the bifurcation point is more clear on the top surface.

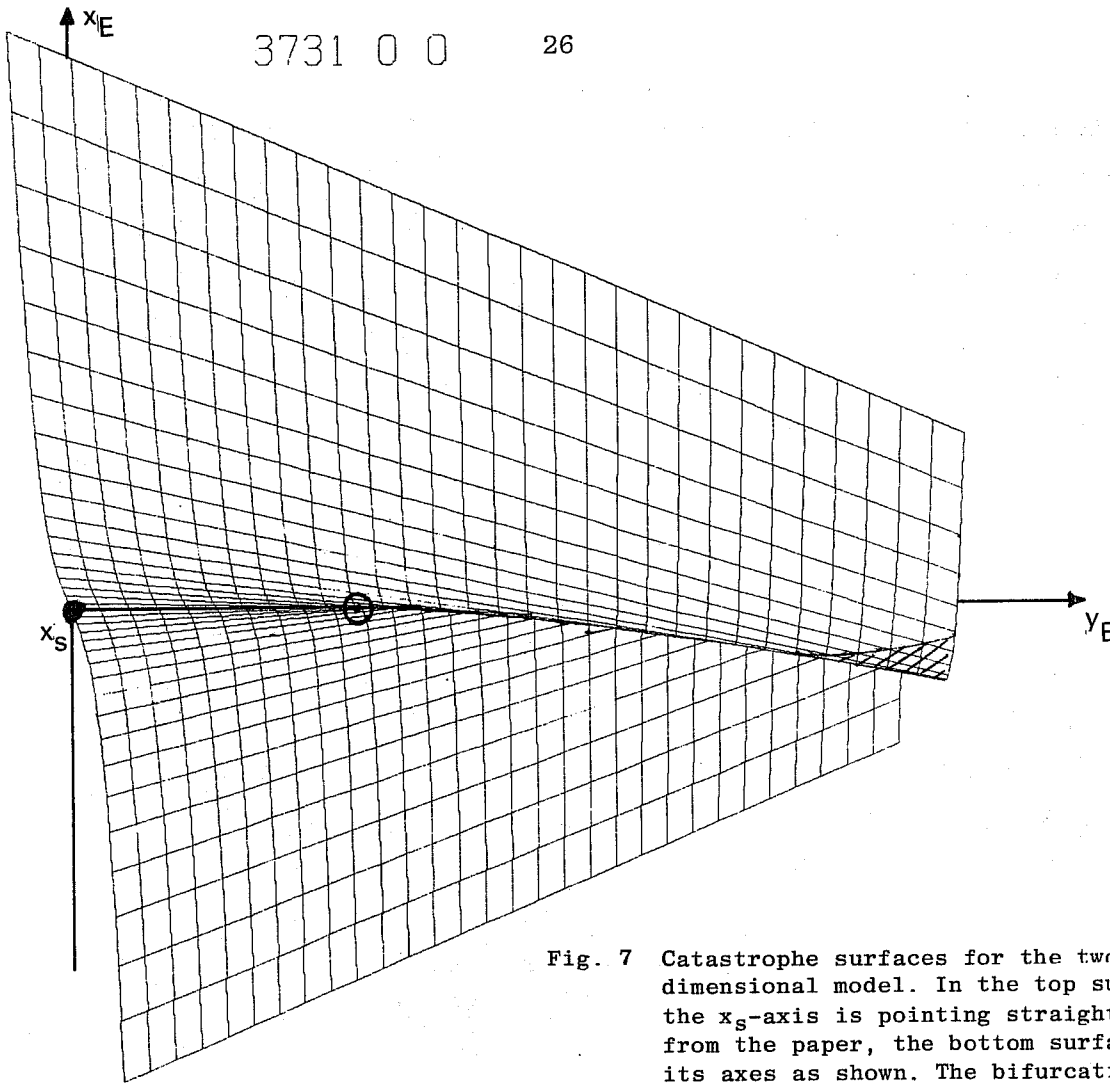

3731135-20

Fig. 7 Catastrophe surfaces for the two-dimensional model. In the top surface the x_S-axis is pointing straight out from the paper, the bottom surface has its axes as shown. The bifurcation point is denoted ⊙ and the hatched area on the top surface corresponds to an unstable steady-state.

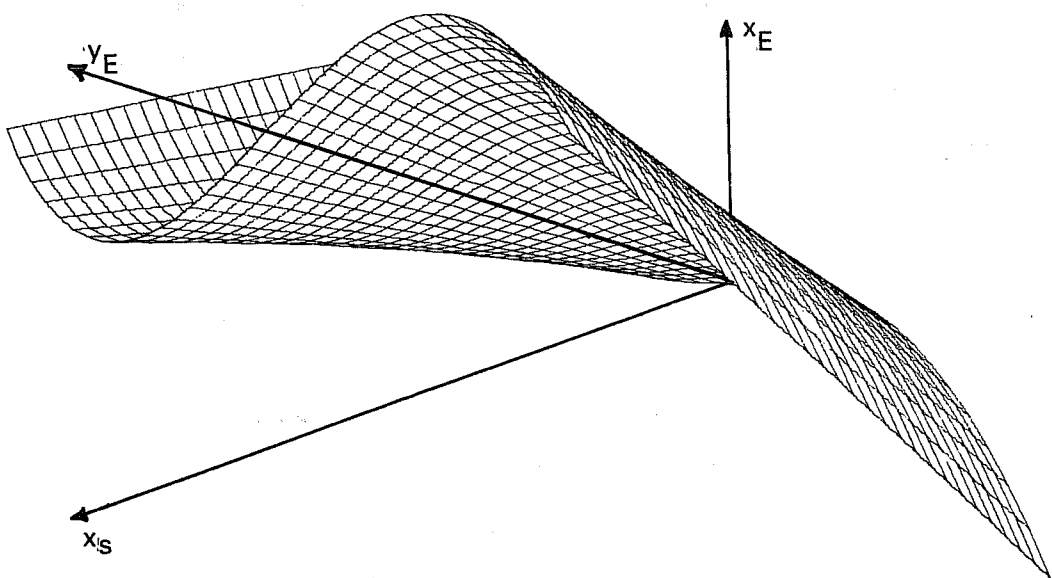

4. A THREE COMPONENT MODEL

The model used in Section 3 may naturally be applied with an arbitrary number of components. The two component model analysed in the previous section will in this section be replaced by a three component model without forcing and dissipation. The purpose is to show the variety of solutions obtained even in this simple case.

The equations for the model are reproduced from Wiin-Nielsen (1975). With the scaling used in this paper they become

$$\frac{dx}{dt} = \frac{1}{2} xy + \frac{1}{2} yz \qquad (a)$$

$$\frac{dy}{dt} = -\frac{1}{2} x^2 + xz \qquad (b) \qquad (4.1)$$

$$\frac{dz}{dt} = -\frac{3}{2} xy \qquad (c)$$

It is seen from the last equation in (4.1) that a steady state must have either $x = 0$, $y \neq 0$; $x \neq 0$, $y = 0$; or $x = 0$, $y = 0$. In the first case we note that (b) and (c) of (4.1) are satisfied and that (a) requires $z = 0$. A steady state is therefore $(0, y_s, 0)$. In the second case we satisfy (a) and (c), while (b) leads to $x_s = 2z_s$. Another steady state is therefore $(2z_s, 0, z_s)$. In the third case we find that all equations in (4.1) are satisfied for an arbitrary value of z_s. The final steady state is $(0, 0, z_s)$. From (4.1) we can furthermore derive the result that $x^2 + y^2 + z^2$ is a conservative quantity for the system (4.1), i.e. the kinetic energy is constant along the trajectory. Without loss of generality we shall in the following select an initial state for which $x_o^2 + y_o^2 + z_o^2 = 1$. In this case we find that the

steady states are:

$$(0, \pm 1, 0), \quad (\pm \frac{2}{\sqrt{5}}, 0, \pm \frac{1}{\sqrt{5}}), \quad (0, 0, \pm 1).$$

Our next goal is to determine the stability of these six steady states. The linearised equations are for an arbitrary steady state (x_s, y_s, z_s)

$$\begin{aligned} \frac{dx'}{dt} &= \frac{1}{2} y_s x' + \frac{1}{2}(x_s + z_s)y' + \frac{1}{2} y_s z' \\ \frac{dy'}{dt} &= - x_s x' + z_s x' + x_s z' \\ \frac{dz'}{dt} &= - \frac{3}{2} y_s x' - \frac{3}{2} x_s y' \end{aligned} \tag{4.2}$$

where the primes indicate infinitesimal deviations from the steady state. We seek solutions to (4.2) of the form $\exp.(\sigma t)$ where σ is the eigenvalue which may be real or complex. In either case, if the real part of σ is positive we will have an unstable steady state. Substitution of this form of solution in (4.2) leads to a set of three homogeneous linear equations. They will have nontrivial solutions if the determinant is zero. This condition leads to the frequency equation

$$\sigma^3 - \frac{1}{2} y_s \sigma^2 + \frac{1}{4}(8 x_s^2 + 3y_s^2 - 2z_s^2)\sigma + \frac{3}{4} x_s y_s (2z_s - x_s) = 0 \tag{4.3}$$

(4.3) is solved for each of the six steady states listed above. The roots of (4.3) are listed below in the six cases:

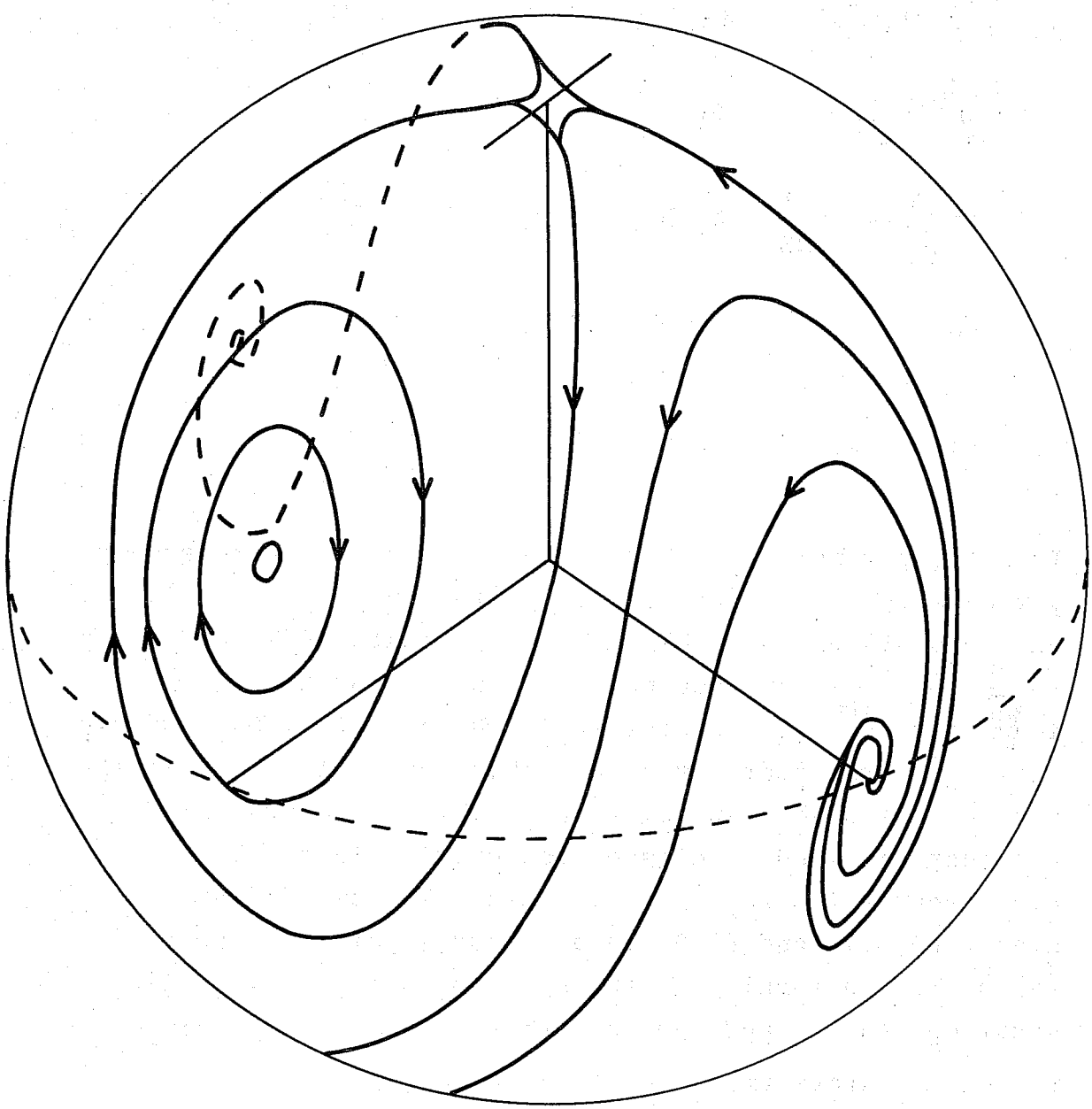

Fig. 8 Trajectories of a three component system without forcing and dissipation. All trajectories are on the surface of the unit sphere. The unstable spiral point in the lower right part of the figure is (0,1,0), while the stable spiral point (dashed curve) on the back of the sphere is (0,-1,0). The neutral point surrounded by trajectories in the left side of the figure is $(\frac{2}{\sqrt{5}}, 0, \frac{1}{\sqrt{5}})$, while the saddle point at the top of the figure is (0,0,1).

$(0,1,0)$: $\sigma_1 = 0, \quad \sigma_{2,3} = \frac{1}{4} \pm \frac{1}{4} i \sqrt{11}$

$(0,-1,0)$: $\sigma_1 = 0, \quad \sigma_{2,3} = -\frac{1}{4} \pm \frac{1}{4} i \sqrt{11}$

$(\frac{2}{\sqrt{5}},0,\frac{1}{\sqrt{5}})$: $\sigma_1 = 0, \quad \sigma_{2,3} = \pm i\sqrt{\frac{3}{2}}$

$(-\frac{2}{\sqrt{5}},0,-\frac{1}{\sqrt{5}})$: $\sigma_1 = 0, \quad \sigma_{2,3} = \pm i\sqrt{\frac{3}{2}}$

$(0,0,1)$: $\sigma_1 = 0, \quad \sigma_{2,3} = \pm \frac{1}{\sqrt{2}}$

$(0,0,-1)$: $\sigma_1 = 0, \quad \sigma_{2,3} = \pm \frac{1}{\sqrt{2}}$

From these results we observe that the only stable steady state is $(0,-1,0)$. The steady states $(0,1,0)$, $(0,0,1)$ and $(0,0,-1)$ are unstable, while the states $(\frac{2}{\sqrt{5}}, 0, \frac{1}{\sqrt{5}})$ and $(-\frac{2}{\sqrt{5}}, 0, -\frac{1}{\sqrt{5}})$ are neutral. The non-zero imaginary part in the states $(0,1,0)$ and $(0,-1,0)$ indicates that the first state is an unstable spiral point while the second is a stable spiral point. The two neutral states are characterised by closed trajectories in the linear case because the real part is zero. The two unstable states $(0,0,1)$ and $(0,0,-1)$ are saddle points. These types apply naturally to the solutions to the linearized equations (4.2), and they are therefore only applicable in the immediate vicinity of the steady state.

The nature of the solutions to the non-linear equations (4.1) is found by numerical integrations of these equations. The general behaviour of the solutions is shown in Figure 8. The trajectories shown in this figure are on the unit sphere. The spiral point in the lower right hand side of the figure is the unstable state $(0,1,0)$. Trajectories starting close to this point will eventually end up in the stable spiral point $(0,-1,0)$ as indicated

by the dashed curve (on the backside of the sphere). The saddle point (0,0,1) is also seen on the figure. The separatrices have been constructed by numerical procedures. Note, in particular, the region to the lower left of the point (0,0,1). Within this region all trajectories are closed curves on the sphere around the neutral point $(\frac{2}{\sqrt{5}}, 0, \frac{1}{\sqrt{5}})$. The region is limited by the closed curve which is made up by a pair of separatrices to the saddle point (0,0,1). A corresponding region surrounds the neutral point $(-\frac{2}{\sqrt{5}}, 0, -\frac{1}{\sqrt{5}})$, but this point is not indicated on the figure. It is thus seen that the surface of the sphere can be divided in three regions: one region surrounds the neutral point $(\frac{2}{\sqrt{5}}, 0, \frac{1}{\sqrt{5}})$. All trajectories inside this region which comes infinitesimally close to (0,0,1) are closed curves on the surface of the sphere. The second region is analogous to the first, but surrounds the neutral point $(-\frac{2}{\sqrt{5}}, 0, -\frac{1}{\sqrt{5}})$. This region comes infinitesimally close to the unstable saddle point (0,0,-1). The third region is the remaining part of the unit sphere. All trajectories in this region will eventually end in the stable point (0,-1,0).

5. CONCLUSIONS

The purpose of this paper is to stress the nonlinear behaviour of the atmospheric systems. We have demonstrated the main aspects of the nonlinear interactions among atmospheric systems of different scales based on data from the northern hemisphere. These results show that any model which is limited to an explicit description of the largest scales of atmospheric motion should include a realistic parameterisation of the interaction between these large scales and the medium and short scales.

The behaviour of the atmosphere on medium and large time scales is of a nonlinear nature. It is likely that the atmosphere for a given forcing and dissipation has a multitude of climatic states. The determination of these states is a difficult problem, and it is significant that all general circulation models result in a climatic state which resembles the present climate. In an attempt to illustrate this problem by particularly simple examples we have analysed the behaviour of some extremely simple nonlinear systems restricted to a few spectral components. For these systems it is relatively straightforward to determine the steady states and to explore the linear stability of these states. The nonlinear behaviour of the systems can be determined by numerical experimentation. Sections 3 and 4 describe the main result of such an analysis. Similar analyses can be found in papers by Wiin-Nielsen (1979), Vickroy and Dutton (1979).

Generalisations from the behaviour of these simple systems to that of the atmosphere is difficult if not impossible. It is nevertheless believed that such analysis may point the way to more general studies of multi-component systems.

References

Chen, T.C. and A. Wiin-Nielsen, 1978 On nonlinear cascades of atmospheric energy and enstrophy in a two-dimensional spectral index, Tellus, 30, 313-322.

Fjørtoft, R. 1953 On the changes in the spectral distribution of kinetic energy for two-dimensional non divergent flow. Tellus, 5, 225-230.

Saltzman, B., 1970 Large-scale atmospheric energetics in the wave number domain, Rev. Geophys. Space Phys, 8, 289-302.

Steinberg, H.L., A. Wiin-Nielsen and C.H. Yang, 1971 On nonlinear cascades in large-scale atmospheric flow, J. Geophys. Res, 76, 8829-8840.

Vickroy, V.G. and J.A. Dutton 1979 Bifurcation and catastrophe in a simple, forced, dissipative quasi-geostrophic flow. J. Atmos. Sci., 36, 42-52.

Wiin-Nielsen, A., 1976 Predictability and climate variation illustrated by a low-order system,Proceedings of Seminar on Scientific Foundation of Medium-Range Weather Forecasts, ECMWF, 258-306.

Wiin-Nielsen, A., 1979 Steady states and stability properties of a low-order barotropic system with forcing and dissipation, accepted for publication in Tellus.

Yang, C.H., 1967 Nonlinear aspects of the large-scale motion in the atmosphere, Ph.D. dissertation, University of Michigan, 173 pp.